Scripta Materialia 113 (2016) 176–179

Contents lists available at ScienceDirect

Scripta Materialia

journal homepage: www.elsevier.com/locate/scriptamat

Regular Article

Mechanical characterisation of hydrogen-induced quasi-cleavage in a metastable austenitic steel using micro-tensile testing

Yoji Mine [a,*], Kaoru Koga [a,1], Oliver Kraft [b], Kazuki Takashima [a]

[a] Department of Materials Science and Engineering, Kumamoto University, 2-39-1 Kurokami, Chuo-ku, Kumamoto 860-8555, Japan
[b] Institute for Applied Materials, Karlsruhe Institute of Technology, Hermann-von-Helmhotz-Platz 1, Eggenstein-Leopoldshafen 76344, Germany

ARTICLE INFO

Article history:
Received 19 September 2015
Received in revised form 3 November 2015
Accepted 10 November 2015
Available online 19 November 2015

Keywords:
Micromechanical characterisation
Austenitic steels
Hydrogen embrittlement
Martensitic phase transformation
Metastable phase

ABSTRACT

Micro-tensile tests were performed using single- and twinned bi-crystals with and without hydrogen pre-charging in a metastable austenitic steel to elucidate the occurrence of hydrogen-induced quasi-cleavage. The hydrogen-charged specimens exhibited in the stress–strain behaviour a stress decrease in the plateau region after yielding. In this stage, a lamellar microstructure of martensite was formed within the parent austenite. Fracture occurred as quasi-cleavage along the habit planes of the martensite lamellae. A mechanism is proposed where the excess hydrogen generated by the martensitic transformation of hydrogen-containing austenite concentrates into the retained austenite between the martensite laths, promoting the localised deformation to fracture.

Austenitic stainless steels are widely used in hydrogen-related industrial applications because of their low susceptibility to hydrogen embrittlement (HE), which depends largely on the stability of the austenitic phase [1–5]. When exposed to gaseous hydrogen at a pressure of 100 MPa, 316L and 310S stable austenitic steels absorb hydrogen at a content of up to approximately 100 mass ppm. Solute hydrogen promotes shear deformation, which results in an extended slant surface in the periphery of the cup-and-cone fracture surface [5]. In this case, 316L and 310S steels, even having such a high content of solute hydrogen, exhibited only moderate decreases in ductility as characterised by a less pronounced reduction of cross-sectional area at fracture. As for the 316 steel with a medium stability of austenite, the specimen containing ~100 mass ppm of hydrogen exhibited a fully shear fracture [5]. Thus, it is reasonable to attribute the hydrogen-induced degradation in the ductility of the stable austenitic steels to a mechanism that involves hydrogen-enhanced localised plasticity (HELP) [6–8].

Quasi-cleavage and flat-faceted features are particularly characteristic of severe HE in metastable austenitic steels with low austenite stabilities, such as 301 and 304 steels [9–13]. The formation of quasi-cleavage may be related with deformation-induced martensitic transformations. Previous studies revealed that cracking in the martensitic phase induced by deformation is responsible for the HE in these steels [13–16]. However, it has been reported that martensite that existed prior to loading was resistant to HE [17,18]. Therefore, the role of martensite in the mechanism of quasi-cleavage in metastable austenitic steels is still controversial. Therefore, it is the main goal of this study to analyse the formation of quasi-cleavage in a metastable austenitic stainless steel from a crystallographic perspective. We employ micro-tensile testing that allows for testing small single crystals and twinned bi-crystals with defined crystallographic orientations.

The material used in this study is a commercial type of 304 stainless steel that is composed of 0.05 C, 18.54 Cr, 8.09 Ni, 0.58 Si, 1.24 Mn, 0.025 P, and 0.003 S (in mass%) with the remainder being Fe. Coarse-grained samples with grain sizes of several tens of micrometres were obtained through solution treatment at a temperature of 1403 K for 2 h followed by water quenching. The coarse-grained samples were thinned to a thickness of less than 30 μm through grinding with emery paper and diamond paste. For electron backscatter diffraction (EBSD) analysis, the surfaces were electro-chemically polished. A field-emission scanning electron microscope (SEM) with an EBSD analyser was used. The EBSD analysis was carried out using the TexSEM Laboratories orientation imaging microscopy software (OIM v. 7.1.0). Single- and twinned bi-crystalline specimens, denoted as SC and TW specimens, respectively, with gauge sections of about 20 μm × 20 μm × 50 μm were fabricated using a focused ion beam (FIB). The loading directions (LDs) for the SC specimen were chosen for single slip as shown in the stereographic triangle in Fig. 1. The TW specimen had a similar orientation and twin boundary parallel to the LD (Fig. 4). A set of specimens in a foil form with gauge part supporting members was soaked in a H_2SO_4 aqueous solution (pH = 3.5) held at a temperature of 353 K and electrochemically charged with hydrogen for 5 h at a current density of 27 A m^{-2}. Based on an estimate of the diffusion velocity [5], the

* Corresponding author.
E-mail address: mine@msre.kumamoto-u.ac.jp (Y. Mine).
[1] Currently: RYOBI LIMITED.

http://dx.doi.org/10.1016/j.scriptamat.2015.11.013
1359-6462/

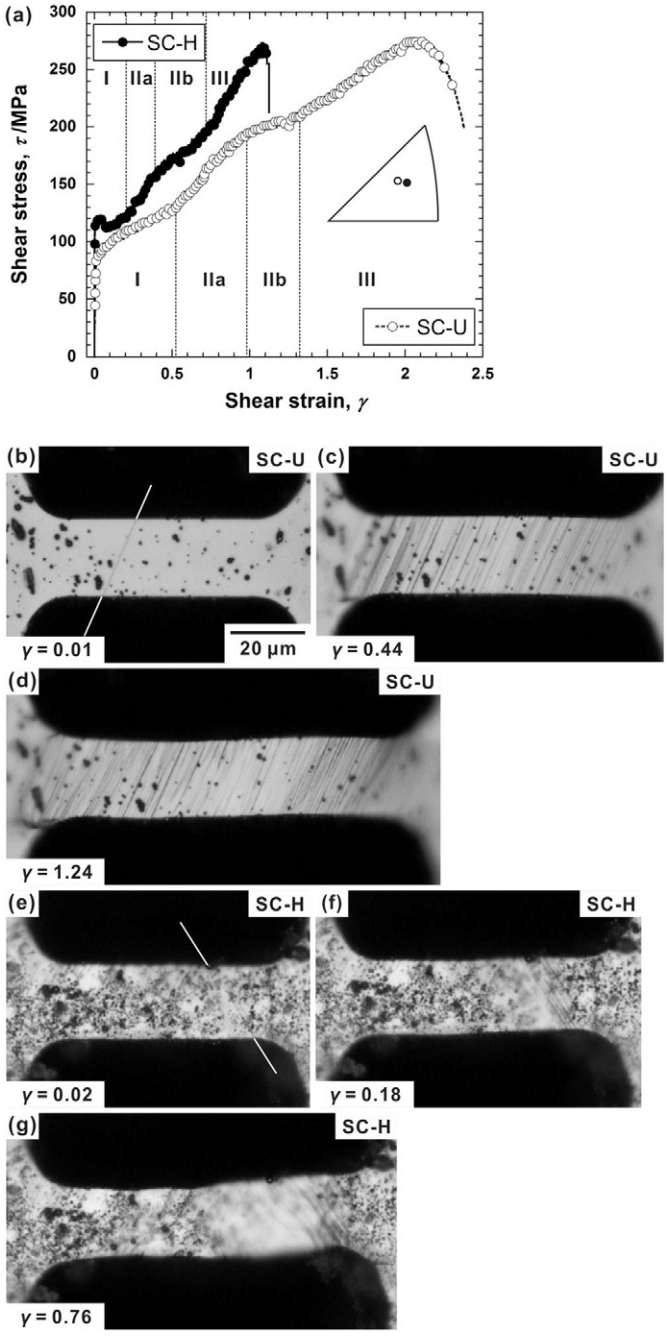

Fig. 1. (a) Shear stress–shear strain curves and (b and c) optical micrographs showing the deformation processes of the uncharged and hydrogen-charged single-crystalline specimens, SC-U and -H, respectively.

charging time was chosen such that the 20 μm-thick specimens are saturated with solute hydrogen. The saturated hydrogen content under the corresponding hydrogen charging conditions was measured to be 101 mass ppm by thermal desorption spectrometry. Tensile tests were started within 3 h after hydrogen charging through cutting the gauge part supporting members using a laser beam. Tensile tests were performed at room temperature under laboratory atmospheric conditions using micro-gluing for gripping and a piezoelectric actuator at a displacement rate of 0.1 μm s^{-1}, corresponding to a strain rate of 2×10^{-3} s^{-1}. The setup has been described in more detail in [19]. The gauge section of the tensile specimen was monitored during tensile testing using an optical microscope in order to dynamically measure the strain as a function of time. For EBSD analysis after failure or after the interruption of loading, the specimens were further fabricated using FIB to make a longitudinal cut. The crystal orientations were determined using automatic beam scanning with a step size of 0.08 μm at an accelerating voltage of 20 kV.

Fig. 1 shows the shear stress–shear strain curves and deformation processes of the hydrogen-charged and uncharged single-crystalline specimens, SC-H and SC-U, respectively. The shear stress and shear strain, τ and γ, were calculated from the nominal stress and strain, σ and ε, using:

$$\tau = \frac{\sigma \cos\phi \sqrt{\varepsilon^2 + 2\varepsilon + \cos^2\lambda}}{1+\varepsilon}, \quad (1)$$

and

$$\gamma = \frac{\sqrt{\varepsilon^2 + 2\varepsilon + \cos^2\lambda} - \cos\lambda}{\cos\phi}, \quad (2)$$

where ϕ and λ are the angles of the LD with the normal of the slip plane and the slip direction, respectively. The SC-U specimen exhibits a three-step work hardening behaviour after yielding at a shear stress of ~79 MPa (Fig. 1a) through the activation of the primary slip system $\{111\}\langle 1\bar{1}0\rangle$ with a Schmid factor of 0.47. This is confirmed by the slip steps that are visible in the optical micrograph in Fig. 1b. The critical resolved shear stress (CRSS) was in agreement with the value obtained by loading in the [111] direction [20]. In the stress–strain curve, a stage I deformation up to a shear strain of about 0.52 can be identified. It is argued that easy glide takes place with the primary slip system being activated (Fig. 1c), although some hardening occurs. When the secondary slip system is activated owing to crystal rotation, work hardening becomes more pronounced (stage IIa) induced through mutual interactions between the dislocations on the two slip systems. The hardening rate is somewhat reduced in stage IIb and, subsequently, the work-hardening rate increases again in stage III. The appearance of the reduced hardening region of stage IIb can be presumably attributed to the formation of martensite, as previously reported by Tsurui et al. [21]. In fact, in-situ observations made during micro-tensile testing of the SC-U specimen revealed that gradual undulation, which differs from slip steps, appeared in region in stage IIb (compare Fig. 1c and d). The increase in the work-hardening rate in stage III can be caused by work hardening of the formed martensite.

While the shape of the stress–strain curve in the SC-H specimen is similar to the one for the SC-U specimen, the stage I is different with a plateau region after the onset of yielding at about 110 MPa, which is 39% higher than that in the SC-U specimen. Overall, the solute hydrogen increases the flow stresses but shortens the length of each stage, resulting in a smaller strain-to-failure. While the trace of the primary slip plane appeared at the onset of yielding (Fig. 1e), the stage I deformation in the SC-H specimen was localised within a short length of the specimen gauge part, as shown in Fig. 1f. In the stage II, deformation was widely spread throughout the entire gauge part through the activation of the multiple slip systems (Fig. 1g).

Fig. 2 compares the fracture morphology of the single-crystalline specimens with and without hydrogen pre-charging. The uncharged specimen exhibits a ductile fracture with strong necking (Fig. 2a and b), whereas the fracture surface of the hydrogen-charged specimen is characterised by a typical hydrogen-induced quasi-cleavage (Fig. 2c and d).

The insets in Fig. 2b and d show the EBSD maps of SC-U and SC-H specimens after fracture, respectively. The analysis reveals that martensite variants developed in both specimens, mainly with their habit planes parallel to the primary slip planes. In the SC-H specimen, variants with their habit planes parallel to the secondary slip plane were also observed (Fig. 2d). This can be induced by plastic constraint at the shoulder part of the specimen. Also, it is confirmed that the quasi-cleavage facets were formed parallel to the two martensite habit planes (Fig. 2c and d).